Fusion Engineering and Design 149 (2019) 111327

Contents lists available at ScienceDirect

Fusion Engineering and Design

journal homepage: www.elsevier.com/locate/fusengdes

Model for a beam driven plasma neutraliser based on ITER beam geometry

I. Turner[a,*], A.J.T. Holmes[b]

[a] United Kingdom Atomic Energy Authority, Culham Centre for Fusion Energy, Culham Science Centre, Abingdon, Oxon, OX14 3DB, UK
[b] Marcham Scientific, Hungerford, Berkshire, RG17 0LH, UK

ARTICLE INFO

Keywords:
Plasma neutraliser
ITER
Negative ions
Halbach

ABSTRACT

A model for a beam-driven plasma neutraliser for a 1 MeV, 40A beam of D^- ions is presented and is based on the dimensions of the ITER gas neutraliser. For the beam-driven plasma neutraliser there is no need for an external power source for producing and sustaining the plasma. Instead the use of high magnetic fields is employed for plasma confinement, which can be produced by arrangement of bar magnets in Halbach arrays around the neutraliser vessel. Magnetic modelling is presented to verify the high cusp fields that can be achieved. The model is an extension of an existing plasma neutraliser model with updated cross-sections, a defined gas profile and magnetic confinement at the entrance and exit of the neutraliser, in order to prevent plasma leakage but still allowing beam propagation with minimal net deflection. The model calculates the beam current fractions and ionisation currents at each step along the length, and at the end of each cycle the induced plasma density and temperature are calculated until convergence is reached. The cusp strength, separation and gas flow rate can be varied and the effects of these parameters on the plasma density and neutralisation fraction are presented. There is currently no data for beam-driven plasma neutralisers therefore possible experiments for benchmarking data are also discussed.

1. Introduction

Neutral beam injection systems (NBI) are under consideration for additional heating and current drive for future fusion machines. For machines such as DEMO and beyond, it is envisaged that approximately 1 MeV beam energies will be required in order to penetrate the plasma. To create neutral beams at such energies requires the neutralisation of negative ion beams as the neutralisation cross-section for positive ions is extremely low. The current method of neutralisation, namely gas neutralisers, can only produce a maximum neutralisation fraction of 58% for negative ion beams at 1 MeV [1] as shown in Fig. 1, and with a wall-plug (electrical) efficiency of approximately 30% depending on beam divergence [2].

The improvement in neutralisation efficiency in using negative ion beams as opposed to positive ions with the same energy however still leads to a low injector wall-plug efficiency as stated above. The wall-plug efficiency, defined as the ratio of launched power to the plasma to the total electrical power consumed by the NBI system, needs to be increased for NBI systems to make a fusion power plant economically viable. Calculations for a plasma neutraliser have shown the required wall-plug efficiency to be 55–60% for a 1 MeV deuterium beam [2] although with a 1.5 MeV beam this can be reduced to 55% [2]. In order to increase the wall-plug efficiency, the neutralisation efficiency can be increased, which can be achieved by the use of plasma neutralisers, i.e. use a plasma in place of neutral gas inside the neutraliser, because the plasma electrons are able to strip the negative ions more effectively.

The conventional method of creating and sustaining the plasma within the neutraliser is to use an external power source [1]. This does not have a significant impact on the power efficiency, however additional complexities are introduced. Therefore an alternative proposed method is to use a beam driven plasma neutraliser, where the negative ion beam passes through neutral gas causing significant ionisation of the gas and hence creating plasma. For this method, there is no requirement for additional power input providing the plasma can be sufficiently confined within the neutraliser, e.g. with magnetic confinement. This makes the beam driven plasma neutraliser an attractive concept.

The power required to form and sustain the neutraliser plasma is derived almost entirely from the energy of the electrons (272 eV per electron for a 1 MeV D^- beam) stripped off a large quantity of the incoming negative ions plus a small amount of double stripping when fast positive beam ions are formed via ionisation of the fast neutrals. For a 1 MeV, 40A D^- beam, this power has been calculated to be ~11kW for the total stripped electron current in the present neutraliser model (42.6A for 5 $Pa.m^3/s$ flow rate at room temperature), and for optimum conversion to a neutral atom beam. The energy of the fast neutrals (and

* Corresponding author.
E-mail address: ingrid.turner@ukaea.uk (I. Turner).

https://doi.org/10.1016/j.fusengdes.2019.111327
Received 8 July 2019; Received in revised form 16 September 2019; Accepted 18 September 2019

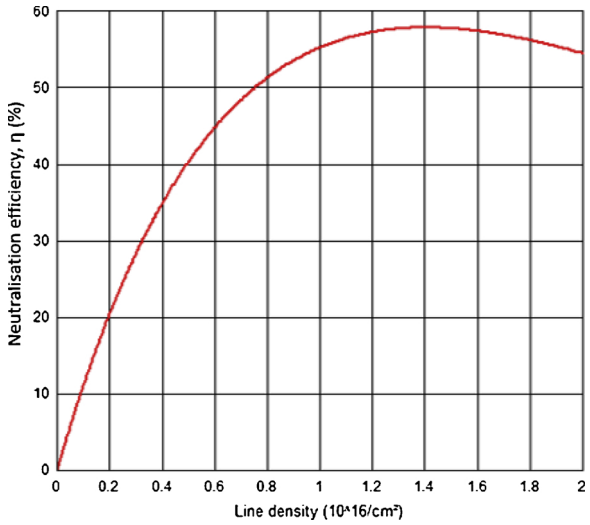

Fig. 1. Plot of neutralisation efficiency vs line density for a D^- beam in a D_2 gas neutraliser at 1 MeV beam energy [3].

positive ions) emerging from the neutraliser is, as a consequence, slightly smaller than the incoming negative ions. There is also a very small contribution to the beam plasma power from the "Rudd" electrons formed by ionisation [4]. This is discussed further in Section 2.3.

Previously the possibility of a beam driven plasma neutraliser had been investigated for a 1 MeV beam by Surrey and Holmes [1] based on a model by Berkner [5]. However this model only applies for a plasma target giving the maximum conversion to D^0 and cannot be tested for non-optimal plasma targets. In this paper, the model by Surrey and Holmes has been developed further and an improved 1D model of plasma generation has been formulated, which also incorporates the neutralisation equations from Berkner [5] but can be applied to any plasma/gas target. It has been used to calculate plasma generation and neutralisation for an ITER-like beam at 1 MeV, using the expected ITER beam profile and the current gas neutraliser dimensions. The model differs from that in [1] in that the inlet flow to the neutraliser is an input variable, which is then used to calculate a gas profile, whereas the original model assumed a flat gas profile. This model also looks in more detail at the magnetic confinement at the ends of the neutraliser as well as along the length, and ANSYS™ has been used to explore magnet arrangements and confirm the optimal cusp strengths and separations that are used as inputs to the model.

2. The model

2.1. Geometry

The dimensions of the plasma neutraliser in this model are based on the geometry of the current design of the ITER neutral beam gas neutraliser, detailed in [6], i.e. a 3 m long, 1.7 m high box divided vertically into 4 channels. The plasma neutraliser design presented here differs from the above in that the channel walls inside the neutraliser box have been removed, because there would not be sufficient space to magnetically confine each channel, given that the expected beam width for each channel is ~80 mm (see Fig. 3 in [6]). Therefore this plasma neutraliser design only has a short duct and orifice at both ends of the box and for each channel, in order to appropriately place column magnets for end confinement of the induced plasma, as illustrated in Fig. 3. We must also consider in the design the plasma exclusion zone surrounding the plasma volume, caused by the magnetic cusps from plasma confinement magnets. This is illustrated in Fig. 2.

It has previously been shown by Hemsworth and Holmes [7] that this distance is ~1.5 times the cusp separation, therefore twice this

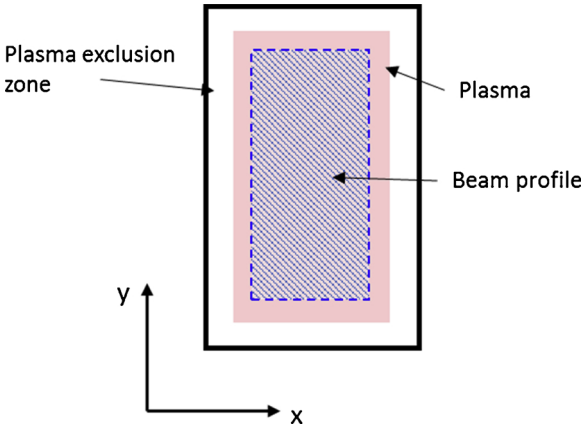

Fig. 2. Simplified cross-section of the plasma neutraliser in the x–y plane illustrating the plasma exclusion zone (drawing not to scale).

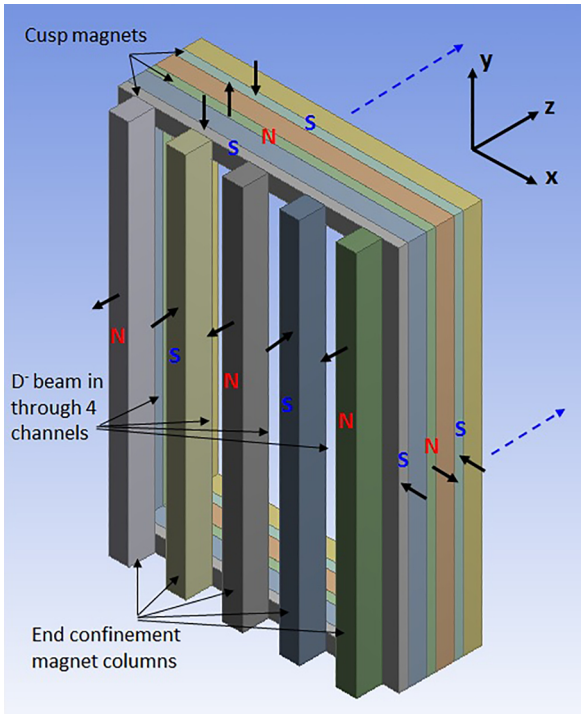

Fig. 3. Small section of a 3D model of the plasma neutraliser showing the beam entrance channels, cusp magnet rings and end confinement magnets. The model is the same at both ends of the neutraliser.

distance must be added to the transverse plasma dimensions in order to calculate the appropriate neutraliser height and width. We do not need to adjust the length of the neutraliser from the ITER design as the beam will need to pass through the end magnet fields at both ends of the neutraliser. Table 1 shows the plasma volume dimensions used in the

Table 1
Plasma neutraliser plasma volume and channel dimensions used for the ITER version of the model.

Dimension	Value (mm)
Plasma length (and box length)	3100
Plasma height	1720
Plasma width	760
Duct length per channel (inner)	60
Duct height per channel (inner)	1600
Duct width per channel (inner)	90

model based on the ITER beam profile:

In Table 1 the length of the plasma neutraliser is slightly larger than the ITER gas neutraliser – this is to allow for an even number of cusp magnet "rings" around the box as will be explained in Section 2.2. In this model we have assumed that the neutraliser gas feed will be in the centre of the length of the box so that the gas flows equally towards both ends. Finer engineering details such as water cooling channels and castellations for securing the magnets have not yet been finalised, as this is outside the scope of this paper. However this would need careful consideration when designing an experiment for benchmarking the model. Fig. 3 shows a small section in 3D of the plasma neutraliser design showing the magnetic arrangement which will be described in more detail in Section 2.2.

Although this version of the model is built specifically for the ITER beam dimensions, it can easily be adapted for a different beamline, such as that now proposed for DEMO [8]. It will also be necessary to benchmark the code against experimental data, therefore future work will include designing a smaller scale test stand experiment to test plasma neutralisation and plasma formation, as discussed later in the paper.

2.2. Magnetic field

A basic linear cusp magnetic arrangement is shown in Fig. 3 and is comparable to that of the JET PINI source [9]. Surrey and Holmes [1] also assumed this arrangement but did not consider the magnet columns at the ends, and assumed an all-round cusp field of 0.5 T. For the model presented in this paper, we consider in more detail end confinement as well as a magnet configuration that generates a higher confinement field along the length of the neutraliser, as a higher cusp field gives higher neutralisation efficiency, as shown in [1]. It was found that this could be achieved by considering the Halbach technique of magnet arrangement [10] and using NdFeB magnets which are stronger than the SmCo magnets used on the JET PINIs, with a remnant induction (B_R) of > 1 T. This arrangement is the same as shown in Fig. 3 but in addition there are interstitial magnets between the north and south cusps, whose magnetisation direction is perpendicular to the north/south cusps. This arrangement creates a strong field on one side of the array and a weak field on the other side, therefore when applied to the neutraliser the strong side would run parallel to the wall. This technique is illustrated in Fig. 4 which shows a simplified 2D arrangement of magnet blocks, representing a cross-section through the magnet cusps.

ANSYS MAXWELL™ has been used to model the Halbach array and confirm the high cusp fields that can be achieved using this method. At first, simple square blocks were modelled as shown in Fig. 4, but it was found that by varying the shape, size and pitch of the magnets, the cusp field (in this case B_y if looking in the y–z plane) could be significantly increased. We need a significantly high field at the cusps (B_y) in order to

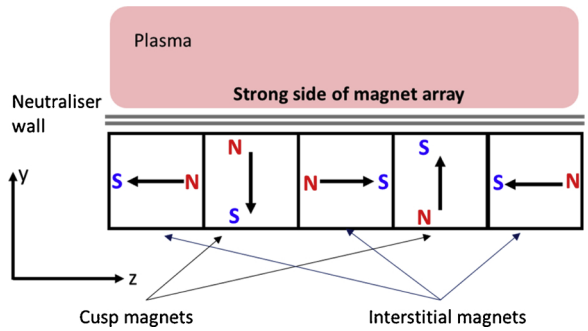

Fig. 4. Simplified drawing of a cross-section through five magnet cusps along the length of the neutraliser (y-z plane) in a Halbach array arrangement. The strong side faces the neutraliser wall.

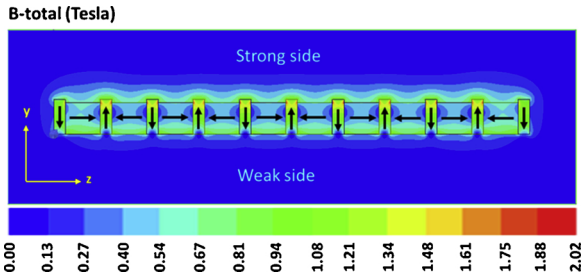

Fig. 5. ANSYS MAXWELL™ map of total B-field generated by a 21 magnet Halbach array using a combination of NdFeB-35 25 mm x 45 mm cusp magnets and 75 mm x 68 mm interstitial magnets giving 100 mm cusp separation. Interstitial magnets also have a 7 mm castellation to account for magnet attachment and water cooling channels.

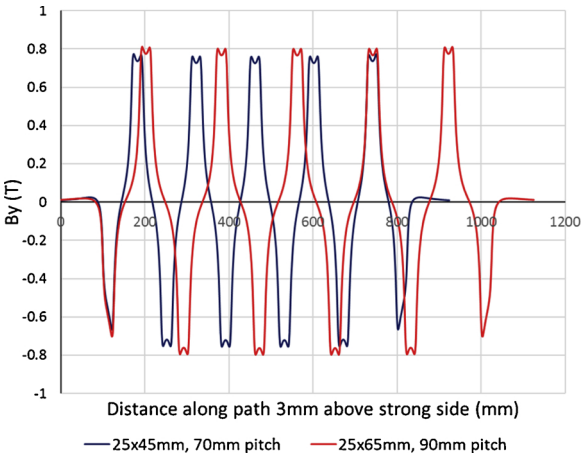

Fig. 6. Cusp field (B_y) 3 mm above strong side of two simulated Halbach arrays with 70 mm and 90 mm cusp separation (pitch).

repel the plasma electrons (similar to the magnetic mirror effect). A visual example of a typical Halbach arrangement is shown in Fig. 5 which also shows the total magnetic field map produced, and the effect of varying the magnet geometry on the cusp field B_y, is shown in Figs. 6 and 7 as simulated by ANSYS MAXWELL™.

Figs. 6 and 7 show that the cusp field can be increased to ≥0.8 T by increasing both the cusp separation and the depth of the interstitial magnets. Ultimately it would be worthwhile to verify the achieved fields experimentally by building a small array of magnets in this arrangement. Finer engineering details will also need to be considered, such as the castellations for water cooling channels and bolting the

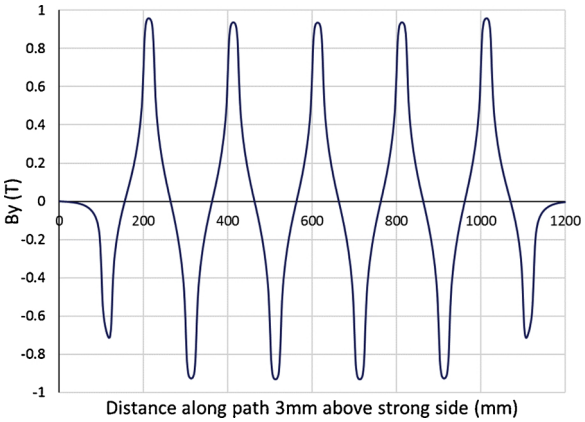

Fig. 7. Cusp field (B_y) 3 mm above strong side of simulated Halbach array with 100 mm pitch, 7 mm castellations and wide interstitial magnets (as in Fig. 5).

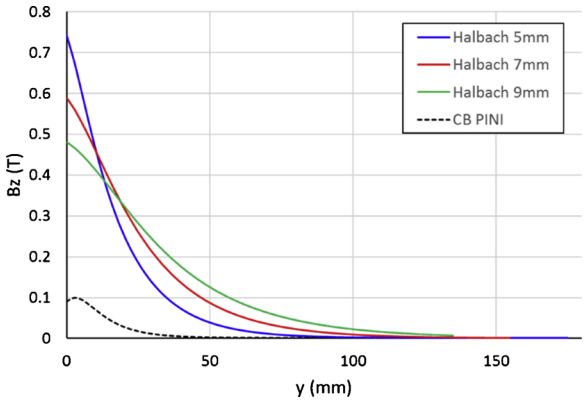

Fig. 8. B_z decay from point between two cusps inwards towards the plasma neutraliser for three different cusp separations in a Halbach array compared to a chequerboard arrangement for a PINI.

magnets in place – some simulations in ANSYS MAXWELL™ to account for these features have already been carried out, for example in Fig. 5, a 7 mm castellation for the interstitial magnets is shown.

An assessment was also carried out to check for any potential leakage of plasma between the cusps (i.e. intercusp losses) compared to the chequerboard PINI source which uses SmCo magnets. This can be done by calculating the line integral of B_z (field parallel to Halbach array) in the y-direction from the midpoint between two cusps outwards towards the plasma neutraliser. Other plasma sources with similar cusp confinement systems to the JET PINI [11,12] have reported low to negligible intercusp plasma losses with a transverse flux similar to that of the JET PINI. This implies that it is very likely that the much stronger intercusp flux of the proposed plasma neutraliser magnet arrangement will have virtually no intercusp losses, despite the vessel's much larger physical size. Fig. 8 shows B_z along the y-direction for 3 different cusp separations in a Halbach array compared to that of a chequerboard PINI (cusp separation = 30 mm), calculated by ANSYS MAXWELL™.

Fig. 8 shows that the integral $\int B_z.\, dy$ is much stronger for large NdFeB magnets arranged in a Halbach array than it is for the chequerboard arrangement with SmCo magnets. We therefore conclude that with the proposed intercusp configuration, plasma leakage is not likely.

Finally we must consider the interaction of the beam with the end magnet fields, as the beam must pass through these in order to enter the neutraliser. The fields of the end magnets and cusp magnets are shown in more detail in Fig. 9.

The transverse velocity v_T acquired by an ion beam passing through an orthogonal magnetic field B_x is given by:

$$v_T = \frac{e}{m}\int B_x dz$$

Conservation of energy requires that:

$$(v_{beam}^2 + v_T^2)\frac{m}{2} = 2eE_{beam}$$

If v_T is equal to v_{beam} then the beam will stall and reverse direction. Thus there is an upper limit on the transverse magnetic field allowed and a practical upper limit for v_T of approximately 0.1 times the axial velocity before the magnetic field is encountered. This limit has been chosen as 0.1 radians is the safe upper limit for paraxial ray calculations – the flux balancing would mean that the displacement in the vertical direction (orthogonal to B) would be approximately 10 mm. Several times this limit would lead to a large upward motion of the beam which would be extremely deleterious. The field created by the bar magnets at the entrance and exit of the neutraliser will simply displace the beam along the entrance slot but will not deflect it as the beam encounters no net magnetic flux, due to the fact that the fields cancel on opposite sides

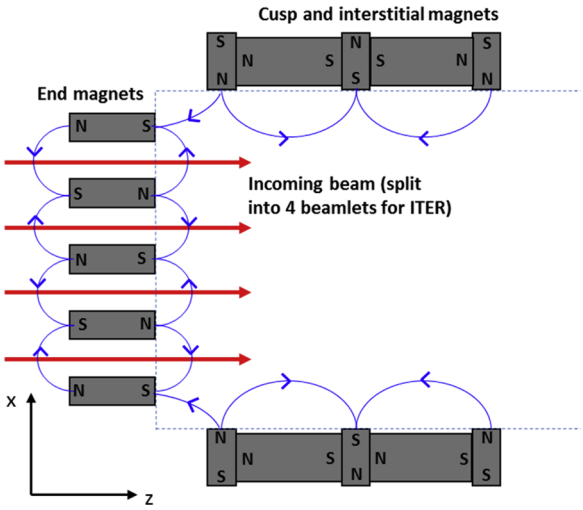

Fig. 9. Sketch of the entrance of the beam into the plasma neutraliser in the x–z plane where z is the beam axis, illustrating the cusp lines of the entrance bar magnets and the Halbach magnets (drawing not to scale).

of the bar magnet. The polarities of the exit bar magnets are reversed because of the even number of magnet cusps along the central region of the neutraliser as shown in Fig. 3. Hence the exiting negative ion beam suffers no net displacement. The double stripped positive ion beam however suffers a double displacement. The value of one displacement S is:

$$S = \frac{2e}{m}\iint B_x dz.\ \frac{dz}{v_{beam}} \approx \frac{2e}{mv_{beam}} B_{xmax}\frac{\delta^2}{2}$$

where δ is the decay distance of the field B_x with axial distance z. If we take B_{xmax} to be 0.2 T and δ to be approximately 0.05 m then the value of displacement S is approximately 1 mm which is small compared to the size of the beam profile.

There is no displacement of the beam from the ring cusp transverse field, as the beam and field vectors are parallel, and the field has to be less than ~0.005 T to not affect the plasma and beam. Fig. 8 shows that depending on the cusp separation, this occurs at 75–120 mm in y for this model, and this is accounted for by the calculation of the plasma exclusion zone.

2.3. The solver

The model of the neutraliser is based on the assumption that every gas molecule that enters the neutraliser from the gas feed (in the middle for this design) has a significant probability of being ionised on its transit to the gas exhaust at either end of the neutraliser. If it is not ionised then the gas density at any point along the neutraliser can be found using the gas flow equations described below. However, if the molecule is ionised then its transit time to the exhaust is increased by the time said molecule remains in an ionised state, which is equivalent to the plasma confinement time. The key requirement for this is that there is no plasma exhaust from the neutraliser volume, that is to say, all plasma ions revert to gas atoms/molecules on the neutraliser walls (at the magnetic cusp lines). No plasma escapes from the neutraliser and recombines elsewhere. This is unlike a conventional ion source where there is a plasma exhaust in the form of an extracted beam.

It is further assumed, for simplicity, that an ionised gas molecule gains no additional advantage in gas conductance after it reverts back to a molecule. This argument is based on the plausible assumption that half of the reformed molecules would be closer to the exit and half further away, so giving no net advantage in gas conductance.

Thus the formation of a fully trapped plasma in the neutraliser does not alter the ambient gas density which is set by the gas flow arguments

described below. However the plasma density is proportional to the plasma confinement time, a geometric quantity which is the plasma volume divided by the product of the cusp loss area and ion sound speed. This can also be described as the time constant for cusp losses once the plasma is established. The ion sound speed is fairly invariant as the electron temperature is usually near 2 eV, as shown in Fig. 15 in Section 3.

The plasma neutraliser model starts by defining the geometry and various input parameters, as well as the collision cross-sections for beam particles with gas, ions and electrons (as used in [5]), and ionisation by heavy particles and electrons. The cross-sections used in [1] have been replaced with up-to-date cross sections from [3] and the IAEA database [13], which are assumed to be the most up-to-date at present. The initial gas density inside the neutraliser box is then calculated using a series of conductance equations for tubes and orifices and assuming molecular flow [14]:

$$\frac{Q}{2} = 9.7\frac{a^2b^2}{(a+b)\left(\frac{L}{2}\right)}\left(\frac{T_{gas}}{M}\right)^{\frac{1}{2}}(P_0 - P_{e1}) \tag{1}$$

$$\frac{Q}{8} = 9.7\frac{c^2d^2}{(c+d)L_2}\left(\frac{T_{gas}}{M}\right)^{\frac{1}{2}}(P_{e1} - P_{e2}) \tag{2}$$

$$\frac{Q}{8} = 3.64A\left(\frac{T_{gas}}{M}\right)^{\frac{1}{2}}(P_{e2} - P_{amb}) \tag{3}$$

In Eqs. (1)–(3), Q is the gas flow rate in litres/second, T is the gas temperature (assumed to be 273 K), M is the molar mass (4 g/mol for deuterium) and P_0, P_{e1}, P_{e2} and P_{amb} are the inlet pressure, exit pressure of the main box to the short ducts, exit pressure from the ducts to the orifices, and the ambient pressure of the surrounding vacuum tank respectively in Pa. These parameters are illustrated in Fig. 10. At present in the model there is no calculation of the gas temperature hence the assumption that it is room temperature, as this would require a more complicated model outside the scope of this paper. This will be the subject of a future paper.

P_{amb} and Q are set by the user and therefore known, hence the equations are used to calculate the two exit pressures and the inlet pressure. The parameters a, b and L in Eq. (1) are the main neutraliser box width, height and length respectively, and similarly c, d and L_2 are the width, height and length of the short ducts at the ends of the box. Finally A is the cross-sectional area of the orifices between the ducts and the surrounding vacuum. The factor of 2 in Eq. (1) arises from the fact that the gas inlet is in the centre of the box causing the gas to flow to both ends equally and therefore the exit pressure is calculated for half the length of the box. Similarly in Eqs. (2) and (3) Q is divided by 8 – this is to account for the fact that there are 8 ducts in total in the system (four at each end) and therefore the flow is divided between them. Despite the inlet being in the centre of the neutraliser, the solver of the code starts at one end of the neutraliser i.e. at the beam entrance, therefore the initial gas density can be calculated using P_{e1}:

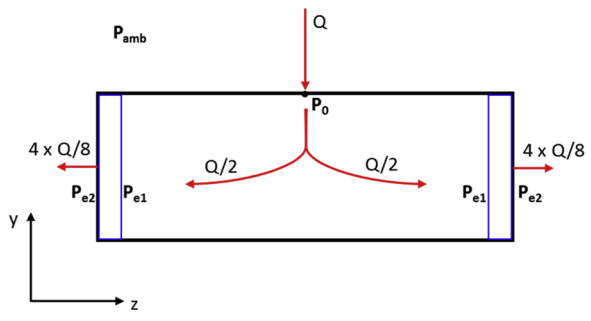

Fig. 10. Sketch of the inside of the neutraliser in the y-z plane showing the various gas pressures in the system and the gas flow rate Q.

$$N_{g0} = \frac{P_{e1}}{k_B T_{gas}}$$

At the very start of the neutraliser, the negative ion current fraction I^- is assumed to be 100% while the positive ion and neutral currents (I^+ and I^0) are set to 0%. As the negative ion beam propagates, some stripping of the D^- ions occurs, resulting in D^0 and D^+ fast ion production in addition to the existing fast D^-. These fast ions undergo various reactions as they propagate causing them to change state, as represented by the Eqs. (4)–(6) from Berkner's paper [5]. Stripping reactions also produce fast electrons (whose current is I_{Strip}), and these along with the three fast heavy particles ionise the background neutral gas.

Ionisation of gas by fast ions produces more fast electrons (hereby known as Rudd electrons [4] with current I_{Rudd}) which cause further ionisation. The fast D^+ ions also cause charge exchange with the gas – this process only produces slow ions with current I_{CX}. These processes are modelled by the following six differential equations which are solved at each step throughout the neutraliser. As a result the three heavy particle currents can be deduced at each step as well as the stripped, Rudd and charge exchange electron currents. The fractional beam currents add to unity at each step, i.e. $I^- + I^+ + I^0 = 1$.

$$\frac{dI^0}{dz} = I^+\sum_S \sigma^S_{+0} n_S + I^-\sum_S \sigma^S_{-0} n_S - I^0\sum_S (\sigma^S_{0+} + \sigma^S_{0-}) n_S \tag{4}$$

$$\frac{dI^+}{dz} = -I^+\sum_S (\sigma^S_{+0} + \sigma^S_{\pm}) n_S + I^-\sum_S \sigma^S_{\mp} n_S + I^0\sum_S \sigma^S_{0+} n_S \tag{5}$$

$$\frac{dI^-}{dz} = I^+\sum_S \sigma^S_{\pm} n_S - I^-\sum_S (\sigma^S_{-0} + \sigma^S_{\mp}) n_S + I^0\sum_S \sigma^S_{0-} n_S \tag{6}$$

$$\frac{dI_{Rudd}}{dz} = I^-\sigma_{i-} n_g + I^0\sigma_{i0} n_g + I^+\sigma_{i+} n_g \tag{7}$$

$$\frac{dI_{Strip}}{dz} = I^-\sum_S (\sigma^S_{-0} + 2\sigma^S_{-+}) n_S + I^0\sum_S \sigma^S_{0+} n_S \tag{8}$$

$$\frac{dI_{CX}}{dz} = I^+\sigma^g_{+0} n_g \tag{9}$$

In Eqs. (4)–(9), the subscript S represents the target species, i.e. neutral gas (g), plasma ions (i) or plasma electrons (e), therefore the summation terms can be expanded to $\sum_S \sigma^S_{ab} n_S = \sigma^e_{ab} n_e + \sigma^i_{ab} n_i + \sigma^g_{ab} n_g$ where a and b represent the charge of the projectile species before and after the collision respectively. It is assumed that the plasma ion density and plasma electron density are equal, which in turn are equal to the plasma density i.e. $n_i = n_e = n_{plasma}$ and therefore the degree of ionisation can be defined as:

$$\chi = \frac{n_{plasma}}{(n_{plasma} + n_g)}$$

On the first pass through the solver, the plasma density is zero because we have not created any plasma before the beam enters the neutraliser. This is calculated after solving the differential equations and is then passed back into the solver in a loop until convergence is achieved. This process is described later in this section.

The three cross-sections in Eq. (7) have a different notation because they represent ionisation of the neutral gas by the three heavy particles D^-, D^0 and D^+. In Berkner's model [5] only Eqs. (4)–(6) are considered, and he neglects all attachment cross-sections. Berkner also assumes a uniform gas pressure profile, hence n_g and n_{plasma} are treated as constants throughout the length. However in our model there is a pressure profile and therefore the gas density is a function of z, which adds to the complexity of solving the differential equations. The plasma density is assumed to remain constant throughout for simplicity as the ionisation rate is almost constant everywhere except at the plasma edge. The impact of non-uniformity will be considered in future modelling

developments using the Epperlein & Haines equations [15]. At intermediate positions along the neutraliser, the pressure is calculated by the following:

$$z < \frac{L}{2},\ P(z) = P_{e1} + \left(\frac{2z}{L}\right)(P_0 - P_{e1}) \tag{10}$$

$$z > \frac{L}{2},\ P(z) = P_{e1} + \left(\frac{2(L-z)}{L}\right)(P_0 - P_{e1}) \tag{11}$$

For simplicity we assume that the pressure drops instantly to P_{amb} on exiting the neutraliser. The gas density at each step can therefore be derived using $n_g(z) = \frac{P(z)}{k_b T_{gas}}$.

The plasma density is calculated at the end of each cycle once Eqs. (4)–(9) have been solved, along with the secondary ionisation currents i.e. from the Rudd and stripped electrons. This zero-dimensional part of the model was initially developed by Holmes [16] and is described here. Firstly the Rudd and stripped electron temperatures (U_x) must be determined, along with their respective confinement times (τ_x) for energy loss:

$$U_R = \frac{2}{3} \times 0.07\sqrt{\frac{E_{beam}}{A}}\quad \tau_x = \frac{V}{U_x\left(\frac{C_e}{B_{ce}} + \frac{C_l}{B_{cl}}\right)}\quad U_S = \frac{2}{3}E_{beam}\frac{m_e}{m_i}$$

In the above equations and as will be applied throughout the paper, the "R" and "S" subscripts stand for Rudd and stripped respectively, and where "x" is used, this implies that the same formula is applied to both Rudd and stripped electrons. In the equation for Rudd temperature U_R, A is the atomic mass of the beam particle (for Deuterium this is 2). The factor of 0.07 is an empirical factor derived from Fig. 13 in reference [4], and has units of $eV^{0.5}$. The factor of 2/3 in the equations accounts for the degrees of freedom of the electrons. E_{beam} is the beam energy in eV, m_e is the electron mass, m_i is the beam ion mass and V is the plasma volume. C and B_c represent the cusp lengths and cusp fields respectively, and the "e" and "l" subscripts differentiate between the end magnets and the main cusp magnets arranged in Halbach arrays respectively. Following this we can then calculated the Rudd and stripped electron densities (n_x) and hence the secondary ionisation currents (I_{x+}):

$$n_x = I_x\left[eV\left(\frac{1}{\tau_x} + \frac{\bar{n_g}K_0\exp\left[\frac{-56}{U_x}\right]}{0.5U_x}\right)\right]^{-1} \tag{12}$$

$$I_{x+} = eVn_x\bar{n_g}\langle\sigma v\rangle_x \tag{13}$$

In Eqs. (12) and (13), e is the electron charge, $\bar{n_g}$ is the average gas density calculated from the pressure profile, and K_0 represents electron energy loss through inelastic collisions ($= 2.4 \times 10^{-12}$eVm^{3}s^{-1}) [17]. The rates $\langle\sigma v\rangle_x$ were derived by Chan [18] for the ionisation of D_2 by electrons.

Finally we are able to determine the plasma density and electron temperature by solving a set of transcendental energy balance equations. Firstly the plasma potential (ϕ) must be determined:

$$\frac{\phi}{T_e} = \eta = \ln\left[\frac{\psi_e(I_R(1-k_R) + I_{R+} + I_{S+} + I_{CX})}{\psi_i(I_R(1-k_R) + I_S(1-k_S) + I_{R+} + I_{S+})}\right] \tag{14}$$

where k_x are the fractions of Rudd and stripped electrons that do not cause ionisation and hence escape directly to the walls:

$$k_x = \left(\frac{1}{\tau_x}\right)\left[\frac{1}{\tau_x} + \frac{\bar{n_g}K_0\exp\left[\frac{-56}{U_x}\right]}{0.5U_x}\right]^{-1}$$

The terms ψ_e and ψ_i are the velocity terms (sound speeds) for plasma electrons and ions respectively:

$$\Psi_e = 0.25\sqrt{\frac{8e}{\pi m_e}}\ \Psi_i = 0.6\sqrt{\frac{e}{2m_{plas}}}$$

where m_{plas} is the plasma ion mass – it is assumed in this model that the plasma is mainly composed of D_3^+ ions, because the probability of D_2^+ ions, formed by electron ionisation, colliding with gas molecules to form D_3^+ ions is very high. An exact ion species calculation has not yet been carried out as it is outside the scope of this paper, therefore we will assume D_3^+ ions – see Fig. 18 in Section 3 for further discussion. Therefore m_{plas} has a value of six times the proton mass. An initial guess for the electron temperature T_e must be made (~1 eV). Then the effective loss area and hence a first estimate for the plasma density can be derived. There are two loss areas in this model due to the two cusp fields. A general equation can be used for both, and the total loss area is simply the sum of these:

$$A_{lossj} = \frac{4C_j}{eB_{cj}}\sqrt{\frac{4m_e\psi_e m_{plas}\psi_i T_e}{0.6}\sqrt{(1+\eta)}} \tag{15}$$

$$A_{loss} = \sum_j A_{lossj}$$

where the "j" subscript represents end losses (e) or losses along the length (l). Hence the plasma density can be written as:

$$n_{plasma} = \frac{[I_R(1-k_R) + I_{R+} + I_{S+} + I_{CX}]}{e\psi_i A_{loss}\sqrt{T_e}} \tag{16}$$

There are three energy sources from which the plasma electrons gain energy: Coulomb drag of primary beam ions, W_b, energy transfer from the Rudd electrons, W_R, and that from the stripped electrons, W_S. The equations for these three energy transfer rates all contain T_e and n_{plasma}, and the sum of the three is equal to the energy removed by escaping ions and electrons:

$$W_b = \frac{3.4 \times 10^{-9}E_{beam}I_{beam}(I^- + I^+)n_{plas}L\sqrt{2}}{E_{beam}^{3/2}v_b} \tag{17}$$

$$W_x = \frac{I_x(1-k_x)n_{plas}k\left(\sqrt{U_x} - 2\sqrt{T_e} - \sqrt{\frac{T_e}{U_x}}\right)}{K_0\bar{n_g}\exp\left[\frac{-56}{U_x}\right] + \frac{2n_{plas}k}{\sqrt{0.5U_x}}} \tag{18}$$

$$W_b + W_R + W_S = T_e[(1+\eta)(I_R(1-k_R) + I_{R+} + I_{S+})] + T_e\eta I_{CX} + T_e I_S(1-k_S) \tag{19}$$

The term "k" is the energy transfer rate between electrons ($=7.7 \times 10^{-11}$m^{3}eV$^{1.5}$s^{-1}) and v_b is the beam velocity. Since T_e is initially guessed, the right hand side of Eq. (19) will not necessarily equal the left hand side, therefore the code alters T_e and returns to Eq. (15) to recalculate the loss area, plasma density and the three energy rates. This process is repeated until the right hand side is equal to left hand side and therefore the true values of T_e and n_{plasma} are derived. The new value of n_{plasma} is returned to the very start of the model to be used in the differential Eqs. (4)–(9), since for the first major cycle there is no plasma present, only neutral gas. The model repeats this major cycle until the plasma density has converged – this is normally very quick with 5 or 6 major cycles and takes a number of seconds to run.

2.4. Neutralisation efficiency

The degree of neutralisation (neutral current fraction) can be calculated at each step in the solver, and the end value determines the overall neutralisation efficiency of the system. However, if the system is not optimised, the efficiency will either not reach its peak value (target is too thin), or it will peak before the end of the length and start to fall (target is too thick). If the length of the system is fixed, then it can be optimised by altering the gas flow Q and/or the beam current. Berkner [5] derived an expression for the maximum achievable neutralisation

efficiency for a given target, which can be applied to any degree of ionisation, by analytically integrating differential Eqs. (4)–(6):

$$\eta_{max} = \frac{\langle\sigma_{-0}\rangle}{\langle\sigma_{-0}\rangle + \langle\sigma_{-+}\rangle}\left[\frac{\langle\sigma_{0+}\rangle}{\langle\sigma_{-0}\rangle + \langle\sigma_{-+}\rangle}\right]^{\frac{\langle\sigma_{0+}\rangle}{\langle\sigma_{-0}\rangle+\langle\sigma_{-+}\rangle-\langle\sigma_{0+}\rangle}} \tag{20}$$

where $\langle\sigma_{ab}\rangle = \sum_S \sigma_{ab}^S \frac{n_S}{n_{tot}}$ and $n_{tot} = \sum_S n_S$. In order to achieve the maximum neutralisation efficiency, there will be an optimum target thickness, which Berkner has also derived [5] and which can again be used with any degree of ionisation:

$$\pi_{opt} = \frac{1}{\langle\sigma_{-0}\rangle + \langle\sigma_{-+}\rangle - \langle\sigma_{0+}\rangle}\ln\left[\frac{\langle\sigma_{-0}\rangle + \langle\sigma_{-+}\rangle}{\langle\sigma_{0+}\rangle}\right] \tag{21}$$

The total integrated target thickness (line density) is given by:

$$\pi = \sum_S \int_0^L n_S dx \tag{22}$$

3. Characterisation and results

To obtain an initial sense of the optimal operating point of the plasma neutraliser, scans were first carried out of cusp separation and cusp field at a fixed gas flow to observe the effect on maximum achieved neutralisation efficiency and target, the results of which are shown in Figs. 11 and Figure 12, 12.

Figs. 11 and 12 show that for a given gas flow rate, increasing the cusp separation and field causes an increase in the maximum achievable neutralisation efficiency and a drop in optimum target required. The same behaviour was shown by the original Surrey & Holmes model [1]. From the magnetic field studies described in Section 2.2, it has been shown that cusp fields of ~0.8 T are comfortably achievable, therefore this value has been chosen for the main cusp field (B_{cl}). Fig. 11 shows that high neutralisation can be achieved by increasing the cusp separation to values over 10 cm, meaning that the neutraliser grows significantly in linear dimensions for large cusp separation due to the plasma exclusion zone (see Section 2.1). Therefore at present an upper limit to cusp separation may be around 150 mm.

It may also be difficult to acquire and handle the large magnets required to produce the high field with such large cusp separations – Fig. 5 shows the magnet sizes that are potentially required for 10 cm separation, which is the value currently used in the model. The neutraliser must have an even number of magnet cusp rings – for an exactly 3 m long neutraliser with 10 cm cusp separation the number of cusp rings would 31, therefore the length has been adjusted to 3.1 m to allow for 32 cusp rings.

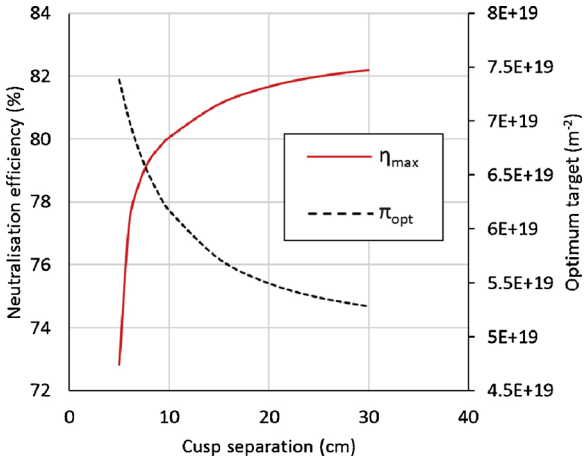

Fig. 11. Cusp separation scan results for maximum achieved neutralisation efficiency and optimum target thickness. Main cusp field set to 0.8 T, inlet flow rate set to 10 Pa.m^3/s.

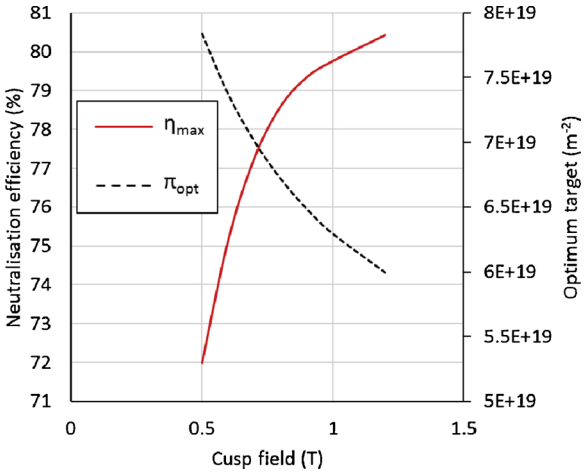

Fig. 12. Cusp strength scan results for maximum achieved neutralisation efficiency and optimum target thickness. Cusp separation set to 7 cm, inlet flow rate set to 10 Pa.m^3/s.

Once the above cusp parameters had been selected, a scan was conducted of gas flow rate as this also has an effect on the target and hence the neutralisation efficiency. This has been done so as to resemble a real system as closely as possible, since achieving a zero-pressure vacuum surrounding the neutraliser would be impossible. The ambient pressure depends on the vacuum pumping speed achievable – considering the design of the ITER NBI cryopumps [19], the external gas density would typically be 5.3×10^{17} m^{-3} which is equivalent to ~0.002 Pa, therefore this value has been used in the model for ambient pressure. Fig. 13 shows the neutral current fraction along the length of the neutraliser at several different flow rates.

Fig. 13 shows that this neutraliser model is optimised between a flow rate of 5 and 10 Pa.m^3/s, as the maximum neutral current fraction (~80%) occurs at the far end where the beam exits the neutraliser within this flow regime. Higher flow rates are shown to cause the maximum to occur at an earlier stage, as well as decreasing its value i.e. at 20 Pa.m^3/s, η_{max} = 78.2%. In theory the neutraliser could be shortened and re-optimised in order to save space. However the gas flow would need to be significantly increased which may not be desirable for pumping. The end cusp effects may also have more of an impact on the beam in a shorter neutraliser. This model has not yet been tested at different neutraliser lengths as it is intended to be a direct comparison with the ITER gas neutraliser, however for a future paper or study this

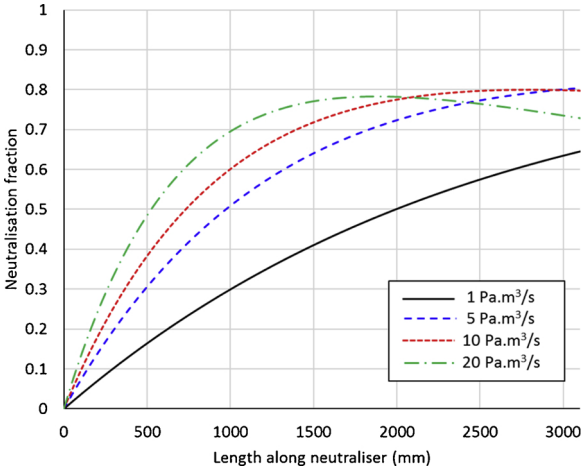

Fig. 13. Neutralisation fraction along the length of the neutraliser at different inlet gas flow rates. Cusp field = 0.8 T, cusp separation = 10 cm, external pressure = 0.002 Pa.

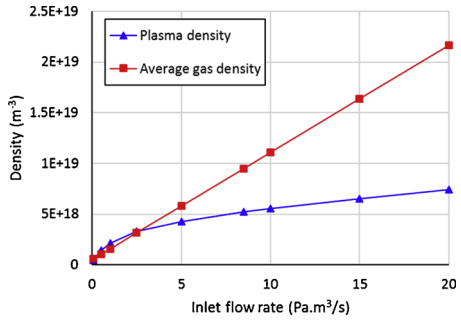

Fig. 14. Plasma density and average gas density variation with gas flow rate. Cusp field = 0.8 T, cusp separation = 10 cm, external pressure = 0.002 Pa.

would be a worthwhile task.

The gas and plasma density variation with gas flow rate is shown Fig. 14, which shows that the average gas density increases linearly with gas flow into the neutraliser as expected but the plasma density (which is also an average) rises more slowly with gas flow as shown. The reason for this can be found by examining Eq. (16) more closely. Of the terms in the numerator of this equation, the ions formed by the stripped electrons are dominant by almost an order of magnitude over the other terms. However this current has a maximum value irrespective of the gas density as once each negative ion is stripped, there is no further production of the stripped electrons, unlike the other currents which do not have this upper limit. The denominator depends on the electron temperature which as seen in Fig. 15slowly decreases with gas flow. Figs. 16 and 17show the variation of the degree of ionisation and neutralisation efficiency respectively. It should also be noted that in Figs. 14–17 there is a small offset to the trends at zero inlet gas flow rate – this is caused by the ambient vacuum pressure, which in turn causes the pressures P0, Pe1 and Pe2 calculated by Eqs. (1)–(3) to also be non-zero.

Fig. 14 shows that an ITER-like beam could potentially produce high density plasmas of the order 10^{18}-10^{19} m^{-3} if the modelling approach presented is correct. Fig. 17 shows that this particular neutraliser is optimal at low gas flow rates (also shown in Fig. 13), which is beneficial as the demand for neutraliser gas is reduced.

4. Discussion

The model presented in this paper has shown that high plasma density and neutralisation can be achieved with a high energy negative ion beam and high magnetic confinement. As a next stage, the model ideally requires benchmarking against experimental results, therefore an experiment needs to be designed with the capabilty of measuring the plasma density as the main objective, since if a plasma of sufficient

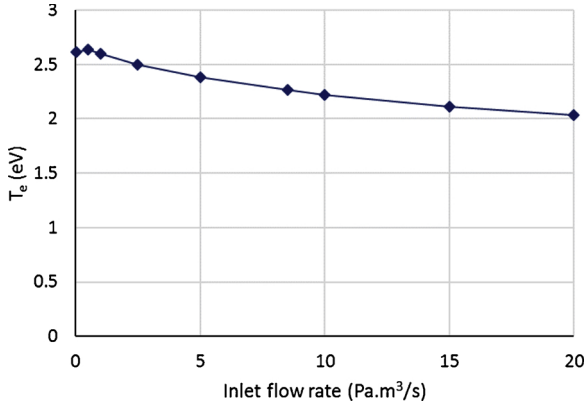

Fig. 15. Electron temperature variation with gas flow rate. Cusp field = 0.8 T, cusp separation = 10 cm, external pressure = 0.002 Pa.

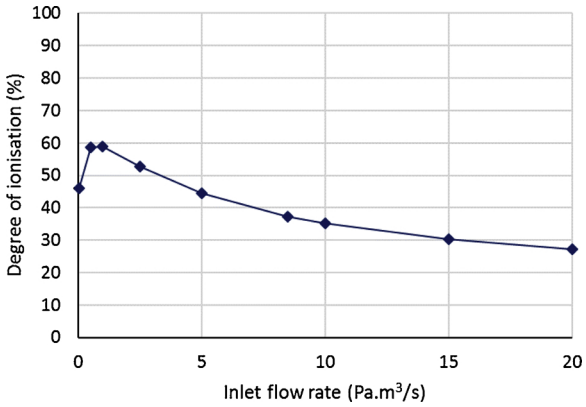

Fig. 16. Degree of ionisation variation with gas flow rate. Cusp field = 0.8 T, cusp separation = 10 cm, external pressure = 0.002 Pa.

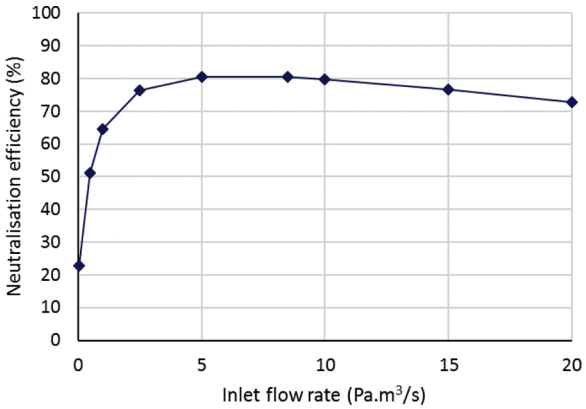

Fig. 17. Neutralisation efficiency variation with gas flow rate. Cusp field = 0.8 T, cusp separation = 10 cm, external pressure = 0.002 Pa.

target density cannot be induced by the beam then there will be no possibility of achieving high neutralisation. At this time no design study has been made to look at the trade off between the neutraliser length and plasma density to achieve optimum design. This has not been done because presently there is no plasma neutraliser injector concept. One factor to consider when designing an experiment is the overall formation time of the plasma, τ_{plas}, since if the experiement uses a pulsed beam and the plasma takes longer to form than the beam pulse duration, then interpretation of experimental results would be much more complicated. This quantity is calculated by:

$$\tau_{plas} = \frac{V n_{plas} e}{I_{ion}}$$

where I_{ion} is the total ionisation current and is equal to $I_{Rudd} + I_{R+} + I_{S+} + I_{CX}$. For a cusp field of 0.8 T, cusp separation of 10 cm and a gas flow rate of 8.5 Pa.m^3/s, this model has a plasma formation time of 24.7 ms. As I_{ion} is proportional to the gas flow and n_{plas} has a slower dependency, τ_{plas} will decrease with gas flow. It would of course be possible to have a scaled experiment provided that there is sufficient target density produced. At present, the possibility of using the Small Negative Ion Source (SNIF) is being considered since this would only require a 2 channel neutraliser of smaller dimensions i.e. length × width × height of approximately 0.4m × 0.4m × 1m, similar to the dimensions of the cylindrical design in [20].

4.1. The plasma ion mass

As mentioned in Section 2.3, it has been assumed in this model that the plasma is mainly composed of D_3^+ ions, although strictly this is unlikely to be the case. The difference in neutralisation fraction caused

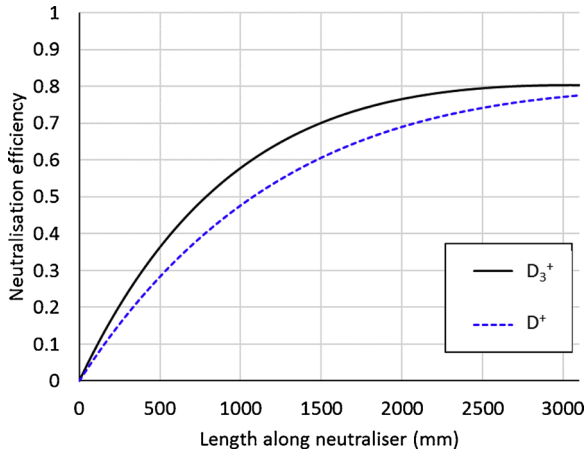

Fig. 18. Difference in neutralisation fraction between using D_3^+ and D^+ ions for the plasma ion mass. Cusp field = 0.8 T, cusp separation = 10 cm, gas flow rate = 8.5 Pa.m^3/s.

by running the model with m_{plas} = D^+ ion mass is shown in Fig. 18.

Fig. 18 shows that there is a significant difference in neutralisation fraction between using D^+ ions and D_3^+ ions as the plasma ion mass. This is something that we aim to investigate as part of further improvements to the model, but will not be done in this paper.

4.2. Plasma neutraliser experiments

The only experiments that have currently been done for plasma neutralisation to date have used plasma neutralisers with external power sources for confinement e.g. arc or microwave driven, hence the need for a new experimental design. An example of an arc driven experiment is detailed in reports by JAERI [21,22], which tested two plasma neutralisers JPN and ONEE. These experiments used linear cusp magnets of similar strength to the PINI magnets and with an argon discharge. Plasma densities of $\sim 10^{17} m^{-3}$ were measured. If the beam-driven plasma neutraliser model presented here is setup in a similar way i.e. cusp strength = 0.25T, cusp separation = 3cm, the plasma density achieved is $3.57 \times 10^{17} m^{-3}$ which is comparable, although the resulting neutralisation fraction is very poor as shown in Fig. 19. This highlights the importance of using Halbach arrays for the magnets and with high cusp fields if beam-driven plasma neutralisation is to be successful.

Finally, when designing an experiment, we must consider the

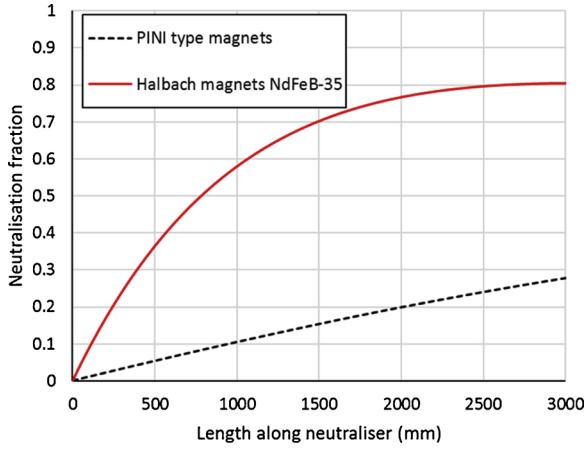

Fig. 19. Difference in plasma neutralisation between using PINI magnets in a linear cusp arrangement and NdFeB-35 magnets in a Halbach array for the current model in deuterium. Cusp field = 0.8 T, cusp separation = 10 cm, gas flow rate = 8.5 Pa.m^3/s.

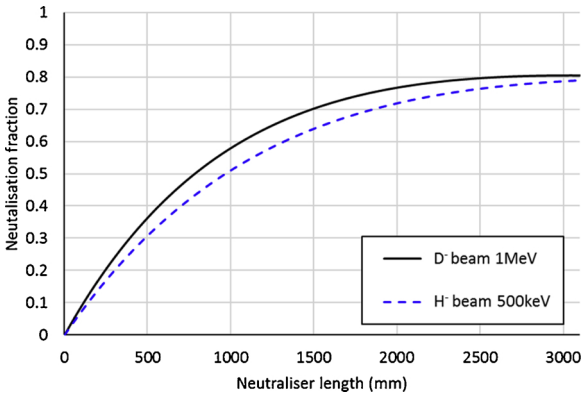

Fig. 20. Difference in neutralization efficiency along the length of an ITER-sized plasma neutraliser between deuterium and equivalent energy hydrogen beams. Cusp field = 0.8 T, cusp separation = 10 cm, gas flow rate = 8.5 Pa.m^3/s for deuterium and 12 Pa.m^3/s for hydrogen.

plasma exclusion zone caused by the cusps, as previously discussed in Section 2.1. Despite the fact that increasing the cusp separation to beyond 10 cm has been shown to increase the neutralisation fraction, this impacts the size of the neutraliser box required, and there is a point where the geometry becomes too large to be practical.

4.3. Application to ITER beams in hydrogen

When ITER first commences NBI operations with the negative ion sources described in [6], hydrogen beams will first be used before deuterium. Therefore if a beam driven plasma neutraliser approach was to be adopted it would be valuable to have prior knowledge of how the system will behave in hydrogen and what changes to operating parameters would need to be made if any e.g. neutraliser gas flow. Fig. 20 shows a comparison of the current model in hydrogen and deuterium. The hydrogen beam was run at 500 keV so that the same cross-sections were used as for the 1 MeV deuterium beam. The gas flow was also increased to √2 times the flow used in the deuterium run, to account for the increased mobility of H_2 gas.

The slight drop in neutralisation efficiency as a result of using hydrogen shown in Fig. 20 can be explained by considering Eq. (16) for plasma density. The loss area calculated by the model for the hydrogen beam is smaller, however this is balanced by the fact that the plasma ion mass for hydrogen is smaller and therefore the value of Ψ_i is larger (2399 for H_2 and 1696 for D_2). Therefore this reduces the plasma density for hydrogen which in turn reduces the value of the stripped electron current.

5. Conclusions

An updated and improved plasma neutraliser model has been presented and is optimised for a 1 MeV ITER-like beam. The neutraliser geometry is similar to that of the current ITER gas neutraliser design, however the model can easily be adapted for a different beamline e.g. DEMO or a test beamline. The possibility of using high magnetic fields for plasma confinement has been investigated and modeled using ANSYS MAXWELL™, and the process is now at a stage where the finer engineering details can be considered. The model can currently achieve neutralisation fractions of at least 80% depending on cusp strength, spacing and gas flow rate, as well as producing high plasma densities.

To further validate the concept, it would be required to compare the model results to experimental data. As there are currently no data for beam-driven plasma neutralisers, an experiment will need to be designed and a neutraliser test stand built, with the capability of measuring the plasma density. It is probable that a smaller scale experiment will be used initially, e.g. approximately 1/3 the scale, therefore the

model will need to be adapted for these purposes. If a negative ion beam cannot be used, it has been shown that high plasma densities are also achieveable with a positive ion beam, and therefore would still serve as a valid test.

Declaration of Competing Interest

The authors declare that they have no known competing financial interests or personal relationships that could have appeared to influence the work reported in this paper.

Acknowledgments

This work has been carried out within the framework of the EUROfusion Consortium and has received funding from the Euratom research and training programme 2014-2018 and 2019-2020 under grant agreement No 633053. The views and opinions expressed herein do not necessarily reflect those of the European Commission.

References

[1] E. Surrey, A.J.T. Holmes, AIP Conf. Proc. 1515 (2013) 532.
[2] R. McAdams, et al., New J. Phys. 18 (2016) 125013.
[3] CCFE cross-section database – ORNL Redbook Atomic Data for Fusion http://www.cfadc.phy.ornl.gov/redbooks/one/1.html.
[4] M.E. Rudd, et al., Phys. Rev. A 20 (1979) 787.
[5] K.H. Berkner, et al., 2nd International Symposium on the Production and Neutralisation of Negative Ions and Beams, (1980).
[6] R.S. Hemsworth, et al., New J. Phys. 19 (2017) 025005.
[7] R.S. Hemsworth, A.J.T. Holmes, Nuclear Eng. 30 (1991) 361–383.
[8] P. Sonato, et al., Nucl. Fusion 57 (2017) 056026.
[9] R.S. Hemsworth, T. Inoue, IEEE Trans. Plasma Sci. 33 (2005) 6.
[10] K. Halbach, Nucl. Instrum. Methods 78 (1970) 185.
[11] K.N. Leung, K.W. Ehlers, Rev. Sci. Instrum. 55 (1984) 342.
[12] K.W. Ehlers, K.N. Leung, Rev. Sci. Instrum. 53 (1982) 1429.
[13] IAEA AMDIS Aladdin database https://www-amdis.iaea.org/ALADDIN.
[14] S. Dushman, Scientific Foundations of Vacuum Technique, 2nd edition), John Wiley & Sons, 1962 Ch 2.
[15] E.M. Epperlein, M.J. Haines, Phys. Fluids 29 (1986) 1029.
[16] A.J.T. Holmes, Plasma Sources Sci. Technol. 5 (1996) 453.
[17] J.R. Hiskes, A.M. Karo, J. Appl. Phys 67 (1990) 6621.
[18] C.F. Chan, et al., Model of Positive Ion Sources for MFE Neutral Beam Injection, Lawrence Berkeley Laboratory Report, 1983.
[19] C. Day, D. Murdoch, J. Phys. Conf. Ser. 114 (2008) 012013.
[20] I. Turner, Eurofusion Report HCD-3.2.4-T003-D001, (2016).
[21] M. Kashiwagi, et al., Development of Plasma Neutraliser using DC Arc Discharge, JAERI-Tech, 2001 2001-046.
[22] Y. Okumura, et al., 5th Joint JA-EU Workshop on Neutral Beam Injectors, (2000).